Designing Low Pressure Turbines for Optimized Airfoil Lift

Jochen Gier
Matthias Franke
Norbert Hübner
Thomas Schröder

MTU Aero Engines GmbH,
Munich D-80995, Germany

In the past 10–15 years, substantial effort has been spent on increasing the airfoil lift especially in aero-engine low pressure turbines. This has been attractive, since increased airfoil lift can be used for airfoil count decrease leading to weight and hardware cost reduction. The challenge with this effort consequently has been to keep the efficiency at high levels. Depending on the baseline level of airfoil lift, an increase of 20–50% has been realized and at least partly incorporated in modern turbine designs. With respect to efficiency there is actually an optimum level of airfoil lift. Airfoil rows at a lift level below this optimum suffer from an excessive number of airfoils with too much wetted surface and especially increasing trailing edge losses. Airfoils at lift levels above this optimum suffer from growing losses due to high peak Mach numbers inside the airfoil row, higher rear diffusion on the airfoil suction sides, and increased secondary flow losses. Since fuel cost have been rising significantly, as has been the awareness of the environmental impact of CO_2, it becomes more and more important to design low pressure turbines for an optimal trade between efficiency and weight to achieve the lowest engine fuel burn. This paper summarizes work done recently and in the past to address the main influences and mechanisms of the airfoil lift level, with respect to losses and efficiency as a basis for determination of optimal airfoil lift selection. [DOI: 10.1115/1.3148476]

1 Introduction

The weight and cost of a low pressure turbine is considerably driven by the airfoil count. In typical low pressure (LP) turbines about half of the module weight is determined by the airfoils. Thus, reduction in the airfoil count directly influences the weight of the turbine component. In addition, lower airfoil count reduces the production and maintenance cost of the turbine. Unfortunately, low airfoil count results in an increased aerodynamic airfoil load. Increasing the airfoil loading too far, however, impairs the efficiency. Since efficiency change in the LP turbine almost directly translates into an equivalent change in engine specific fuel consumption ($1\%\ \Delta\eta \rightarrow 0.5\text{–}0.9\%\Delta$SFC) any efficiency penalty has to be thoroughly traded with the weight and cost benefits. In blades this has to be done with special care due to stress issues in the circumferentially extended shrouds of high lift airfoils.

Zweifel [1] was the first to link aerodynamic load and efficiency with the aim of determining the optimal pitch to chord ratio. He introduced a lift coefficient, known nowadays as the Zweifel number, which is widely used to characterize the aerodynamic load of an airfoil row. Further important work in the understanding of the flow in LP turbines with their transitional boundary layers was done by Emmons [2] and Schubauer and Klebanoff [3], who discovered the calmed regions following turbulent spots. The transitional character of turbomachinery boundary layers and especially in LP turbines has been already investigated in the 1970s and 1980s. e.g., by Walker [4], Hodson [5], Hodson et al. [6], and Halstead et al. [7–10].

Usually high lift airfoils are referred to having Zweifel numbers larger than 1. Actually, some LP turbine designs in engines, such as the V2500, which entered service in the late 1980s, already have airfoil rows with Zweifel coefficients in the order of 1 or somewhat higher. A better understanding of the underlying flow effects were investigated by Hoheisel et al. [11] in 1987. They investigated a family of three LP turbine cascades T104–T106. This family includes airfoils with both front and aft loading having values of the Zweifel coefficient, Z, of about 1.04–1.07. The fundamentals of aero LP turbine design with the background of these investigations are described by Hourmouziadis [12]. The T106 airfoil has been widely used especially in Europe in several variants for research on LP turbine boundary layers.

In 1982 Pfeil et al. [13] already experimentally investigated the influence of unsteady wake impingement on the laminar-turbulent transition in boundary layers. Further fundamental work on this topic was reported by Hodson [14], Schulte and Hodson [15], Banieghbal et al. [16], and Stadtmüller et al. [17].

Besides a lot of other work on a better detailed understanding of the boundary layer behavior in LP turbine-typical cascades some work was reported on the introduction of high lift or ultra-high lift (depending on the baseline and definition) into LP turbines.

Gier et al. [18] investigated differences between moderate and high lift second vane in a three-stage LP turbine using transitional computational fluid dynamics (CFD) for analysis. Gier and Ardey [19] investigated the mechanism for the increasing loss due to high lift. Based on this combined with radial rig traverse data, Ardey and Gier [20] investigated the effect of high lift on the 3D flow and the related losses.

Haselbach et al. [21] and Howell et al. [22] introduced two high lift levels into the three-stage LP turbine of the BR710/715 family. They reported that the Reynolds number lapse rate, hence efficiency drop at lower Reynolds numbers, was significantly stronger for the so-called ultrahigh lift design with Zweifel numbers in the area of 1.1–1.2.

Some new very high lift airfoils were tested in cascades often with incoming wakes. Houtermans et al. [23] put additional focus on the separation prediction of high lift airfoils. Coton and Arts [24,25] added heat transfer measurements to loss and transition investigations in a high lift airfoil. Popovic et al. [26] tested two airfoils with extremely high Zweifel numbers in the area of 1.4 in a low-speed cascade, and Praisner et al. [27] investigated the performance improvement potential of contoured endwalls. Lazaro et al. [28] took a close look into the loss production mechanism in a low-speed cascade with moving bars.

A large amount of work has also already been carried out with the focus on boundary layer control by different kinds of transition triggering. MTU published a patent in the mid-1980s with a

Contributed by the International Gas Turbine Institute of ASME for publication in the JOURNAL OF TURBOMACHINERY. Manuscript received September 1, 2008; final manuscript received April 1, 2009; published online March 25, 2010. Review conducted by David Wisler. Paper presented at the ASME Turbo Expo 2008: Land, Sea and Air (GT2008), Berlin, Germany, June 9–13, 2008.

specially shaped boundary layer trip [29]. Sitaram et al. [30] investigated the effect of cylindrical elements of different diameters at various chordwise positions on an impulse blade and achieved loss reductions of up to 16%. Volino [31] used rectangular bars of different heights and at different locations and presented correlations for determining optimal bar heights. Ramesh et al. [32] proposed to combine both unsteady and surface roughness in an optimal way. Zhang et al. [33] and Vera et al. [34] investigated passive turbulation devices to be applied on the airfoil suction side in order to suppress large separation bubbles present in high lift airfoils in a low-speed and a high-speed facility, respectively.

Another way of inducing transition is the use of active boundary layer control. For this, usually steady or pulsed injection is investigated. Examples are Bons et al. [35], Sondergard et al. [36], Volino [37], and McAuliffe and Sjolander [38].

The purpose of the present work is to summarize the impact of airfoil lift variation on loss mechanisms and their intensity in real turbines. Therefore, the main loss sources with connection to airfoil load are first discussed using cascade examples. In a second step three test turbines are discussed and evaluated with respect to efficiency impact of lift variation. The final assessment then discusses the overall path for choosing optimal airfoil lift levels.

2 Zweifel Lift Coefficient

The so-called Zweifel coefficient is the most widely used dimensionless parameter for characterization of the airfoil load level. It was introduced in 1945 by Otto Zweifel working for BBC [1]. It is based on the idea of comparing the actual loading and the "ideal" loading being defined by the pressure difference between the inlet stagnation pressure and the exit static pressure by their ratio. Pullan and Harvey [39] provided a nice drawing and deduction of the Zweifel number *Z*. This deduction is similar to the original one but with a different flow angle convention (from axial instead of circumference). For a flow on a streamsurface it is given by

$$Z = \frac{\text{actual loading}}{\text{ideal loading}} = \frac{P\rho V_m (V_{\Theta 2} - V_{\Theta 1})}{c_m (p_{01} - p_2)} \tag{1}$$

The normal deduction assumes constant meridional velocity V_m and incompressibility. With $V_2 = V_m / \cos \alpha_{m2}$ the Zweifel coefficient can be written as

$$Z = \frac{P\rho V_m^2 (\tan \alpha_{m2} - \tan \alpha_{m1})}{c_m 1/2 \rho V_2^2}$$

$$Z = 2\frac{P}{c_m}\frac{(\tan \alpha_{m2} - \tan \alpha_{m1})}{\sec^2 \alpha_{m2}} \tag{2}$$

This formulation includes a couple of important simplifying assumptions. As mentioned above it is assumed that the meridional velocity, hence the axial velocity in purely axial configurations, is constant. The second important assumption is incompressible flow. For compressible flow with Mach numbers in the mid- to higher subsonic regime, which is typical for real LP turbines, Eq. (1) should be written

$$Z = \frac{P \cdot (\rho_2 V_{m2} V_{\Theta 2} - \rho_1 V_{m1} V_{\Theta 1})}{c_m (p_{01} - p_2)} \tag{3}$$

In the case of constant density and constant V_m, this equation collapses again to Eq. (1). Introducing the continuity equation into the numerator of Eq. (3) results in

$$Z = \frac{P}{c_m} \cdot \frac{\rho_2 V_{m2}^2 \left(\tan \alpha_2 - \frac{V_{m1}}{V_{m2}} \cdot \frac{A_{m2}}{A_{m1}} \tan \alpha_{m1} \right)}{(p_{01} - p_2)} \tag{4}$$

The term $(p_{01} - p_2)$ is higher than the incompressible dynamic pressure for increasing Mach numbers, e.g., by about 10% for Ma=0.6. This relationship can be directly deduced and is only a function of Ma and gas constant γ. The expression in the brackets in the numerator, however, is a function of Ma number and flow path. This influence depends on the case. For example, in a turbine with compressible flow and $V_m \approx$ const., the area ratio A_{m2}/A_{m1} has to be larger than 1, adding to the numerator for typical LP turbine velocity triangles. This discussion should not devaluate the Zweifel number. Zweifel himself described only a partially compressible formulation [1]. But one should be reminded that comparisons of Zweifel coefficients have to be done with some care.

3 Loss Characterization in High Lift Airfoils

Loss generation in turbines is a very complex combination of a number of mechanisms. In attempts to describe, separate, and quantify the different influences on loss, Traupel [40] and Denton [41] provided in-depth assessments based on comprehensive survey of existing data. Although the influences interact to a certain degree, the total aerodynamic loss in an airfoil row is usually split into two categories—two-dimensional (2D) and three-dimensional (3D) losses. Two-dimensional losses sum up the individual loss sources of the boundary layer flow around the airfoil, while the three-dimensional losses characterize the losses occurring primarily in the proximity of the endwalls at the hub and tip.

In low pressure turbines with their usually high aspect ratio airfoils, the 2D losses contribute significantly to the overall loss. Main source of these losses is the dissipation taking place inside the airfoil boundary layer. Most of this dissipation is coming from the airfoil suction side due to its high Ma number level and usual rear diffusion. In addition losses are generated at the trailing edge due to the back pressure losses.

Denton [41] tried to separate different components of 3D loss in an airfoil row. According to his assessment more than half of the 3D losses are caused by the boundary layer flow on the endwalls including the platforms upstream the leading edge and especially downstream of the trailing edge. As a second source he points out the mixing of the inlet boundary layer amplified by the secondary flow. A third component according to Denton is related to secondary kinetic energy (SKE), which can contribute in the order of 25% of the 3D entropy generation. There may be further entropy generation components related, e.g., to transition changes due to interaction of secondary flow with blade surface boundary layer flow.

To assess the influence of the airfoil lift level on loss, these model considerations are evaluated with respect to the influence of blade lift.

3.1 Influence on 2D Losses. As mentioned above the main driver for the 2D losses is the entropy generation in the boundary layer flow around the airfoil. Denton [41] provided a relation for the total entropy generation

$$\dot{S} = \sum_{\text{PS+SS}} C_S \int_0^1 \frac{C_d \rho V_0^3}{T} d\left(\frac{x}{C_S}\right) \tag{5}$$

where the summation is for both the suction and the pressure side. This can then be used to formulate an entropy generation coefficient ζ_s

$$\zeta_s = \frac{T\dot{S}}{m \cdot 0.5 \cdot V_{\text{ref}}^2} \tag{6}$$

Combining these two equations Denton comes up with the following expression for an entropy generation coefficient:

$$\zeta_s = 2 \sum_{PS+SS} \frac{C_S}{P \cos(\alpha_2)} \int_0^1 C_d \left(\frac{V_0}{V_2}\right)^3 d\left(\frac{x}{C_S}\right) \tag{7}$$

It should be noted that this formulation has the underlying assumption of low-speed flow. However, the principal relationship is

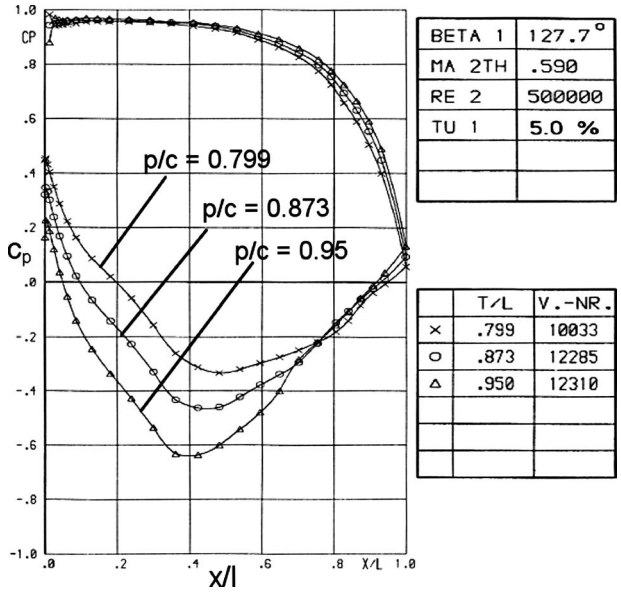

Fig. 1 Pressure coefficient in T106 cascade for 3 pitch: chord ratios (A, B, and C) [42]

the same for compressible flow.

The most important point in relation to airfoil lift is the term $(V_0/V_2)^3$. Assuming the dissipation coefficient c_d is known and does not vary too much, this velocity term causes the suction side boundary layer flow to contribute the largest part to the loss generation. Increasing the airfoil lift directly translates to increased velocity levels on the suction side for similar pressure distribution families.

In Fig. 1 a comparison of the pressure distribution is plotted for the widely used family of T106 airfoils. The T106 has been designed for a pitch to chord ratio of 0.799 (T106 A) and two larger spaced versions; B and C had been defined and tested with about 10% and 20% increased pitch. However, these airfoils have not been redesigned for the same exit flow angle as T106 A, leading to somewhat reduced turning for these two airfoils.

Taking a look into a potential specification of an aerodynamically optimal airfoil lift one can find diagrams for optimal pitch to chord ratios in turbines in the book of Traupel [40] and the paper of Denton [41]. They are plotted in Fig. 2. The flow angle conventions in the two diagrams are different with Traupel using angles with respect to the circumference and Denton using angles with respect to the axial direction. Knowing or assuming a stagger angle the pitch to chord ratio can be converted into a pitch to axial

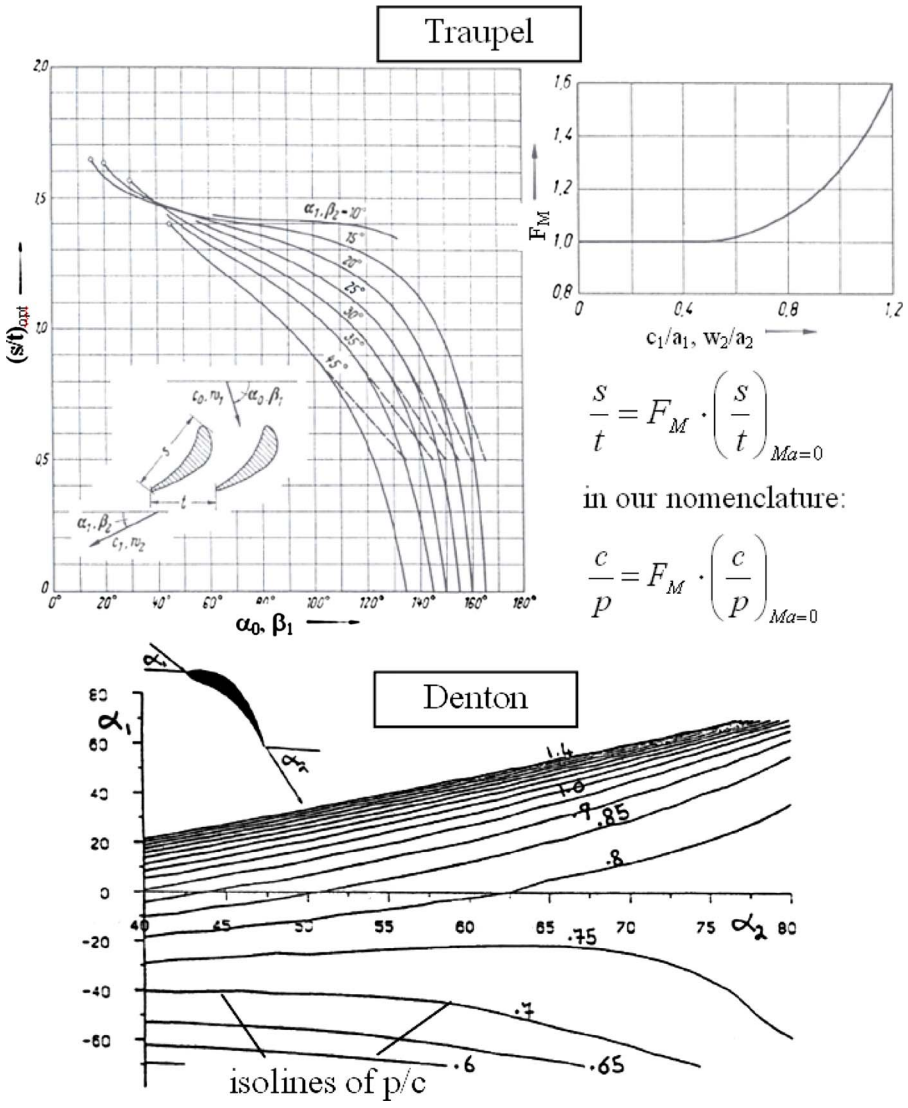

Fig. 2 Diagrams for optimal pitch to chord ratio from Ref. [40] top and from Ref. [41] bottom

Table 1 Comparison of airfoil lift coefficients for T106 family

	α_1	α_2	p/c	β_s	p/c_{ax}	Z
T106A	−37.7	63.1	0.799	30.7	0.93	1.04
T106B	−37.7	61.9	0.873	30.7	1.02	1.19
T106B (α_2 as A)	−37.7	63.1	0.873	30.7	1.02	1.14
T106C	−37.7	60.6	0.95	30.7	1.10	1.36

chord ratio, which is the input into the Zweifel coefficient definition. Assuming an axial flow path for simplicity an optimal Zweifel coefficient can be computed from

$$\frac{P}{c_{ax}} = \frac{P}{l \cdot \cos \beta_s} \tag{8}$$

$$Z = 2\frac{P}{c_{ax}} \cdot \frac{\tan a_2 - \tan \alpha_1}{\sec^2 \alpha_2} \tag{9}$$

Unfortunately both relationships for optimal p/c deviate from each other quite considerably for a couple of boundary conditions. For the T106, for example, with the flow angles and stagger angle printed in Table 1 Traupel provides an optimal p/c including the compressibility correction of 1.02, while from Denton's diagram one can extract a value for an optimal p/c of 0.73. This is a huge difference.

In order to get some idea about p/c magnitudes in a typical LP turbine airfoils, the widely used cascade family T106 is used. The T106 A has a p/c of 0.8, which can be viewed as moderate high lift (Table 1). Going beyond p/c of 1 as the optimal choice indicated by the Traupel diagram for this airfoil is really ultrahigh lift and cannot be expected to be optimal.

The T106 family consists of four variants, from which three are chosen for discussion in this paper. The version D with a p/c of 1.05 is omitted, since its loading is too extreme. It is important to note that the pitch to chord increase for the B and C versions has been achieved by simply increasing the pitch distance without modifying or restaggering the airfoils. This inevitably leads to a reduction in exit flow angle. An overview is given in Table 1.

Table 1 has four lines. In lines one, two, and four, the three cascade versions A, B, and C are given with their respective real exit flow angles. From the data in the table the Zweifel coefficient according to Eq. (9) is computed in the right column. In line three the sensitivity for the Zweifel number with respect to exit flow angle is displayed by using the exit flow angle of the baseline A version. It can be seen that the T106 A already has an elevated Zweifel number level above 1.0. The two versions B and C have an increased airfoil load of about 10% and 20%, respectively. Comparing the p/c of the baseline version A with the correlation for optimal p/c this airfoil can be expected to be somewhere in this optimal region. The versions B and C are then located at an increased lift level, which could be expected to correspond to increased loss.

Traupel [40] and Denton [41] both provided a relation for the optimal p/c ratio, but they do not describe a function of loss for p/c ratios deviating from this optimum. However, the entropy loss coefficient definition given by Denton can be used to estimate the loss impact of airfoil load with respect to the 2D boundary layer flow.

For this the measured pressure coefficient is plotted for the three cascades T106 A, B, and C in Fig. 1. The data come from testing the airfoils in a high-speed cascade (DFVLR Braunschweig, cascade now in University of Armed Forces, Munich) [42]. In this figure an operating point at a Reynolds number of 500,000 is chosen to avoid a significant influence of a separation bubble at this point. The grid-induced free-stream turbulence was 4%. Denton's formula (7) does a summation of pressure and suction side, where due to its mostly much smaller free-stream velocity level, the pressure side losses turn out to be much smaller. Applied in an approximate way to the T106 family one can compare its result with the measured 2D loss, which is reported in Table 2.

In the first column an average value for cp is read out of Fig. 1 with the assumption of $cp_{avg}=0.6\ cp_{max}$ as approximation. An average isentropic Ma number can be computed from this. Since we have compressible flow, we use this Ma number to compute its third power and reference this to the value of the baseline version A (third column). A value is added for the pressure side, which is only marginally affected by the lift variation (column 4). This value is then divided by the pitch and then again referenced to the T106A value, giving the increase in the loss coefficient with the lift increase. When compared with the last column with the measured loss coefficient change (Fig. 3), a reasonable match can be detected.

Of course this estimation has limited generality, since it involves a couple of assumptions. One major assumption is that there is a constant diffusion coefficient c_d. Therefore the estimation above has been done for a high Reynolds number in the absence of separation bubbles. In reality, the diffusion coefficient is not constant in an LP turbine boundary layer. Especially the transitional behavior of the boundary layer has a significant impact on the diffusion coefficient and thus the entropy generation.

Increasing the lift of an airfoil row directly leads to an increase in the area in the pressure distribution. This is characterized by the Zweifel coefficient. Since the free-stream velocity on the pressure side is usually already low except for the last 10% of the chord, this load increase is realized by lower pressure on the suction side like in the example of the T106 family (Fig. 1). This can be done by either loading up the front part of the suction side pressure distribution and by increasing the peak Ma number, hence decreasing the minimum pressure.

In any case there is the additional effect of an upstream move of the throat area on the suction side for larger pitch to chord ratios. These characteristic changes lead to an increase in the diffusion of the suction side boundary layer between minimum and exit pressures, both in terms of pressure difference and surface length. One measure to limit this is by modifying the pressure distributions

Table 2 Comparison of loss estimation based on free-stream velocity with measured loss coefficient

	Cp_{avg}	Ma_{is} avg.	$(Ma/Ma_{T106A})^{\star\star 3}$	Sum PS+SS	$(\zeta_s)/(\zeta_s)_{T106A}$	ζ (Re=500 k), measured	ζ/ζ_{T106A} measured
T106A	−0.192	0.655	1.0000	1.2200	1.0000	1.9200	1.0000
T106B	−0.285	0.685	1.1471	1.3670	1.0256	1.9200	1.0000
T106C	−0.384	0.718	1.3169	1.5369	1.0595	2.0200	1.0521

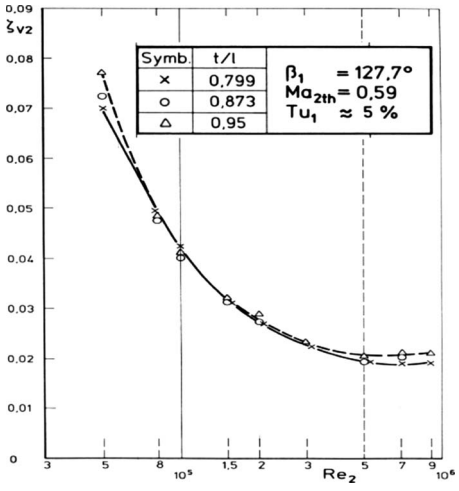

Fig. 3 Loss coefficient in T106 cascade (midspan) for three pitch: chord ratios (A, B, and C) [42]

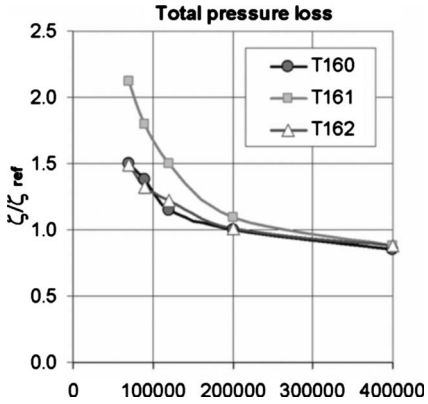

Fig. 5 Comparison of loss coefficient at midspan for baseline (T160) and two high lift cascades (T161 and T162), inflow with wakes

characteristic by increasing front loading.

In a more recent investigation than the T106 airfoils two new high lift airfoils (T161 and T162) have been designed and compared with a baseline airfoil (T160). The tests were performed in the high-speed cascade facility of the University of the Armed Forces, Munich. Their pressure distributions are shown in Fig. 4. In contrast to the T106 family, the two high lift airfoils have been designed for the same velocity triangle as their baseline T160. The T160–T162 airfoils have a turning close to 110 deg with an acceleration ratio of only 1.6, which is realized by a divergent flow path in the cascade. Thus, these airfoils have a higher turning and lower acceleration than the T106.

The Zweifel coefficient for the T161 and T162 is identical at nearly 1.2 and about 25% higher than for the T160. The main difference between T161 and T162 is the different types of the pressure distribution. T161 features a pronounced rear loading with the peak suction being at the same axial chord as for baseline. T162 in contrast is more forward loaded with a smaller deceleration gradient after peak suction. The computed pressure distributions compare quite well with the experiment and exhibit the same trends. All computations in this paper have been performed with the CFD code TRACE developed at DLR and used as in-house code within MTU [43].

In Fig. 5 the resulting losses at midspan are plotted as a function of the Reynolds number. The tests have been performed with a moving bar at the inlet to simulate incoming wakes and for realistic flow Mach numbers. It can be seen that the form of the pressure distribution has a significant impact on the performance especially at low Re numbers. The T162 has a very comparable loss at midspan to the baseline T160, hence thinking in terms of Eq. (7), the higher Ma number level on the suction side is compensated by the reduced surface and reduced number of trailing edges. The rear loaded T161 in contrast features a steeper Re lapse rate, what could be expected for this profile type with reaching a similar loss for relatively high Re numbers.

Summarizing the discussion of 2D losses, it can be noted that the introduction of higher lift in an airfoil row leads to increased losses through the elevated Ma number level of the free-stream close to the suction side and the longer and more pronounced suction side diffusion. This longer diffusion results in an earlier laminar-turbulent transition and longer turbulent boundary layer portions. Hence, the diffusion coefficient in Eq. (7) is higher on average. There is a balancing mechanism due to reduced surface area and fewer trailing edges incurring back pressure related losses. However, after surpassing some lift level in the order of Zweifel >1 the additional loss mechanisms start to become progressively larger even in the absence of an open suction side separation.

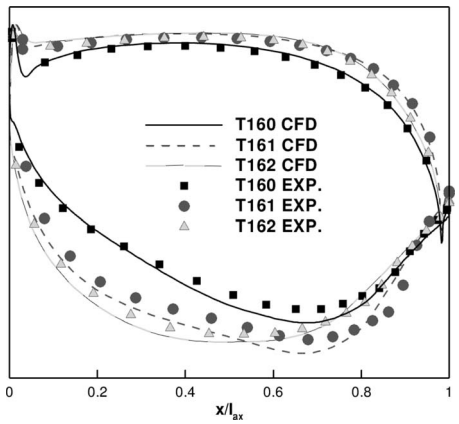

Fig. 4 Pressure distribution for baseline (T160) and two high lift cascades (T161 and T162), Re=200k, with periodic wakes at inlet

3.2 Influence on 3D Losses. In contrast to the 2D losses, the publication of Denton [41] does not provide any relation for loss as a function of blade load. Traupel, however, provides a formula, which is linearly dependent on the pitch to airfoil height ratio

$$\zeta_{\text{rest}} = \frac{\zeta_p}{\zeta_{p0}} F \frac{p}{h} + \zeta_a \quad \text{or} \quad \zeta_{\text{rest}} = \frac{\zeta_p}{\zeta_{p0}} F \frac{p}{c} \cdot \frac{c}{h} + \zeta_a \tag{10}$$

The ratio of ζ_p to ζ_{p0} is the ratio of the profile loss (2D) to the basic profile loss and is usually close to unity. For the function F Traupel provides a diagram, where F is a function of turning and acceleration. For a given height h of the airfoil, an increased parameter pitch p—by airfoil count reduction—gives a linearly increased loss coefficient. However, this formula has to be used with care, since p/c and the aspect ratio are combined here.

Denton [41] tried to segregate the individual contributions to 3D loss. The first major endwall loss source he addresses is the loss generated in the endwall boundary layer. Together with the platforms upstream of the leading edge, and especially downstream of the trailing edge, this loss could be responsible for up to 2/3 of the total endwall loss according to Denton.

Assessing the question, which influence an increased lift level could have on this loss component, one can use the idea of Eq. (7) again. As discussed above, an increased airfoil lift leads to increased local Ma number levels on the airfoil suction side and its proximity. Thus this elevated Ma number level also exists on the

endwall boundary layer. Even if it is assumed that the diffusion coefficient c_d does not change, compared with a lower lift airfoil there are regions of higher Ma number in the endwall boundary layer free-stream. These introduce additional losses without any intensification of the endwall secondary flow structures. This loss increase grows gradually with increased airfoil lift

The second loss mechanism described by Denton [41] is mixing loss of the inflow boundary layer, which is amplified by the secondary flow. The third component is the loss associated with the secondary kinetic energy SKE, which is said to be about $\frac{1}{4}$ of the total endwall loss. Due to the complexity of the secondary flow, there is no reasonable relationship known to deterministically characterize the different influences of the global parameters on these secondary flow mechanisms, hence none for airfoil lift.

However, one could do a simple thought experiment. Assuming an airfoil row with an extremely small pitch to chord ratio, thus, very small lift, the radial penetration height of the secondary flow motions will be pretty small. It cannot be expected that the size of the vortices significantly exceeds the distance between suction and pressure side. There is not much inflow vorticity per airfoil passage for such a small pitch, which then can roll up and cause mixing losses downstream. In case of an enlarged pitch the amount of vorticity per passage increased naturally and so the vortical structures like the passage vortex system can move further into the flow channel. Although not quantifiable this can be expected to increase the endwall loss, too.

To get an idea of the intensity of these effects the total pressure losses of the three cascades T160–T162 are compared in a plane downstream of the trailing edge for the same Reynolds and Mach numbers (Fig. 6). The results support the reasoning in the last paragraph. The core of the passage vortex indicated by the maximum in total pressure loss coefficient has moved from about -0.39 rel. channel height z/h to about $z/h=-0.36$ for T161 and to $z/h=-0.35$ for T162, respectively. Thus the two high lift cascades exhibit the expected move of the secondary flow system toward midpassage.

The two high lift cascades both seem to have higher losses than the baseline airfoil. To assess this more quantitatively, the integral losses of these three cascades are separated into 2D and 3D losses. The 3D losses are calculated from the integral loss minus the 2D loss. This loss breakdown is compared with the result for the "rest" loss ζ_{rest} in correlation (10) [40] in Fig. 7.

It can be seen that both high lift cascades exhibit higher overall losses than the baseline T160. Although the 2D loss of T162 is almost identical to that of T160, its 3D loss is significantly higher. For the rear loaded T161, the 3D loss is only moderately increased. However, its 2D loss exhibits a significant increase, at least at this Re number, leading to a significant overall loss increase. Since the correlation of Traupel does not take into account any airfoil design variables, such as stagger angle, besides the height and pitch, it computes identical 3D losses for the high lift cascades. If one roughly averages the 3D loss of the two high lift airfoils from measurement and compares it to the predicted (correlation) loss increase, both are pretty similar with a value of 0.2 $\zeta_{\text{ref-T160}}$. This result is in line with recent findings of Zoric et al. [44] who compared a front loaded and an aft loaded high lift airfoil with the baseline PAKB cascade airfoil.

Finally, the radial distribution of the secondary kinetic energy computed from the experimentally gathered velocities is shown in Fig. 8. As expected, the intensity of the SKE is increased for both high lift designs compared with the baseline. Their distribution and maximum is quite comparable. The higher 3D loss of the T162 compared with the T161 cannot be explained by differences in the SKE. This is in line with Fig. 6, where the differences in flow structure between the more aft loaded T161 and the more forward loaded T162 are relatively small. The stronger 3D loss of the T162 seems to originate significantly from the region at about 25% span ($z/h=0.25$). This could be an interaction with the airfoil boundary layer, which increases due to the longer deceleration length of the forward load design.

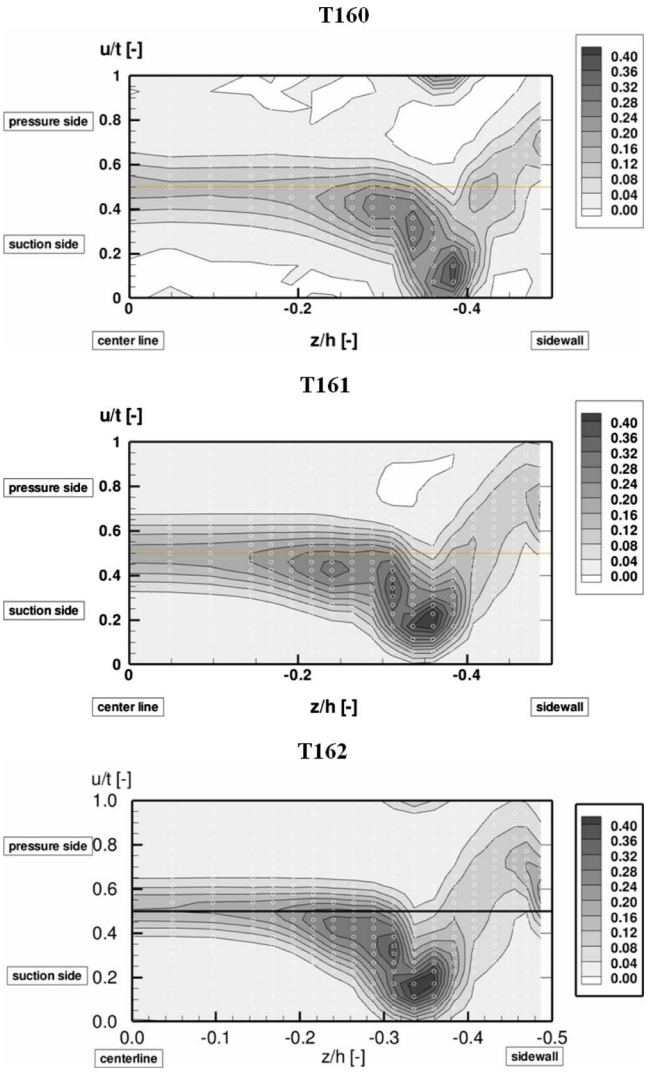

Fig. 6 Total pressure loss for baseline (T160) and two high lift cascades (T161 and T162) 40% downstream of the trailing edge

There is a mentionable influence of the airfoil lift on the loss in an airfoil row. Actually the 3D losses can contribute quite significantly to the lift-related loss increase (Fig. 7). The discussed cascade tests indicate that their contribution may well be larger than the contribution from additional 2D losses. In any case the 3D

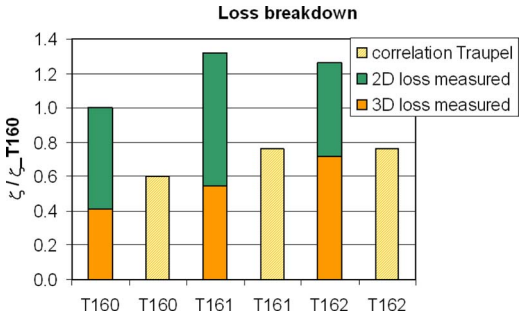

Fig. 7 Total pressure loss (reference T160 total loss) for baseline (T160) and two high lift cascades (T161 and T162), Re =200k

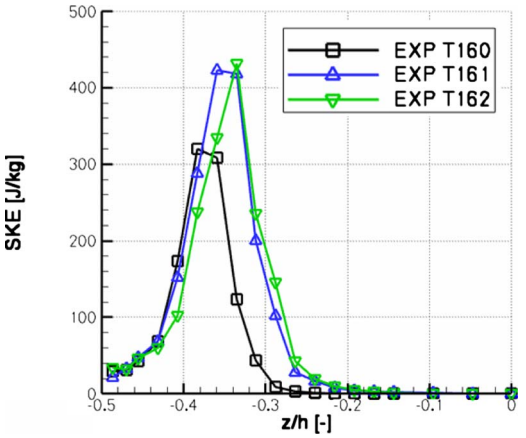

Fig. 8 Secondary kinetic energy comparison between T160 and two high lift cascades, T161 and T162, Re=200k, half span

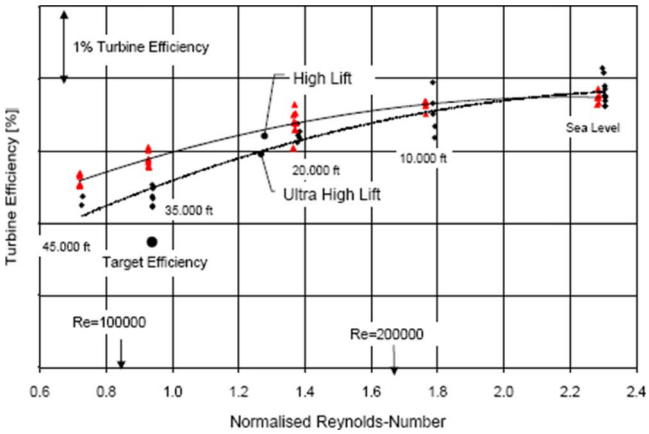

Fig. 9 Turbine efficiency versus normalized Reynolds number for HL and UHL blading from Ref. [21]

losses will also gradually grow with airfoil lift increase, pushing any aerodynamic lift optimum toward reduced Zweifel numbers.

4 Evaluation of Lift Variation in Turbines

In real turbines two main issues have to be addressed. The first is the performance impact of lift variation, which for LP turbines is primarily characterized by the efficiency development in the operating map and the sensitivity to Reynolds number, hence flight altitude level. The second issue is the evaluation of what causes an efficiency change in the full turbine. In analogy to Sec. 3 this could be a change in 2D boundary layer losses, as well as 3D losses, with all the complex interactions of the real machine.

In this paper three LP turbines are evaluated and discussed to at least a certain degree. All have been tested as real speed full scale turbine rigs in an altitude test. The first turbine is a Rolls-Royce design based on the BR715 and has been published by Haselbach et al. [21]. The second is an older MTU design (MTU-A) three-stage LP turbine. The third is a more recent MTU design (MTU-B) five-stage LP turbine. For all described turbines the discussion is based on a comparison of at least a high lift with a more or less conventional design.

The BR715 LP turbine described by Haselbach et al. [21] is a three-stage turbine for a midsize aero-engine. The comparison of Haselbach et al. is based on a lift increase of 11% for the so-called "ultrahigh lift" design from the baseline BR715. This lift increase was incorporated in the second and third stage, while the first stage remained unchanged. The turbine has a high aspect ratio of 4–5 typical for LP turbines. It should be also noted that the airfoils were made thinner on the pressure side, with local thickening in the endwall proximity to suppress the interaction of secondary flow with pressure side separation bubble.

In Fig. 9 the overall performance of the two builds is compared as a function of Reynolds number, thus flight altitude. The Re variation is sufficient to cover the range between take-off and high altitude. As also highlighted by Haselbach et al. [21] the ultrahigh lift turbine has a stronger Re lapse rate, leading to no efficiency drop at take-off (sea level) and 0.5% efficiency drop at cruise Re numbers at around Re=120,000.

Also, it is important to note that Haselbach et al. reported a significant sensitivity of the efficiency change with the revolution speed in the operating map between 100% and 120% speed. The efficiency drop was smaller for a higher speed of 120%. Haselbach et al. [21] gave two reasonable explanations for this phenomenon. First, the flow turning in the airfoil rows is reduced for higher speeds. This is expected to damp the intensity of the secondary flow and reduces especially the 3D loss. Since high lift airfoils tend to increase 3D losses as also shown above, the benefit of the higher speed is larger for these airfoils. Second, the higher turning velocity leads to higher wake frequencies, which are generally reduced for high lift with fewer airfoils per row. Haselbach et al. [21] referred to similar effects in the cascade experiments. However, a change in wake frequencies in a cascade experiment performed in a way as described by Haselbach et al. also changes the average turbulence level in the airfoil row. And the individual wakes produced by high lift airfoils are stronger and with more turbulence than wakes of lower lift airfoils.

The second rig in the discussion is referred to as MTU-A turbine rig. Figure 10 shows a picture of the general arrangement. The baseline turbine build D01 is deduced from the first three stages of a large turbofan engine. Three configurations are compared and discussed. The first is the baseline build D01, which had been built up with three different sectors in the second vane with different airfoil loading designs. Here, the baseline with 138 vanes and the high lift version with 111 vanes are used. A plot of the pressure distribution of the second vane in build D01 is shown in Fig. 11. It is taken from an earlier paper of Gier et al. [18]. The type of the pressure distribution is maintained with the typical effects of higher peak Ma numbers and a forward shift of peak suction due to the larger pitch to chord ratio.

The third configuration is called build D02, which is the build shown in Fig. 10. Here, all stator rows are equipped with airfoils with 20% higher loading. The rotor rows also had been redesigned but with unchanged airfoil count. All build D02 airfoils feature additional 3D design measures.

In Fig. 12 the efficiency of the three configurations is compared for two speed lines. For the design speed (n/n_d=100%) the conventional lift build D01 shows and efficiency advantage of about 0.3% compared with the high lift build D02. Within the measure-

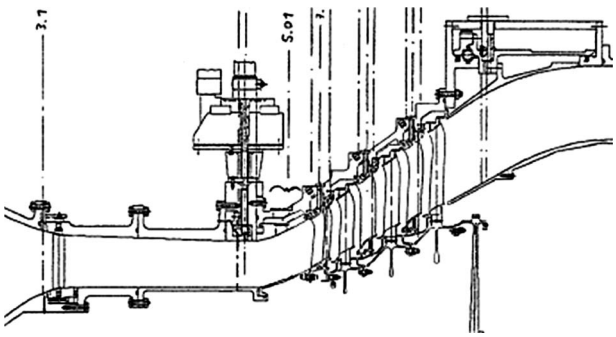

Fig. 10 General arrangement of MTU-A turbine rig, build D02

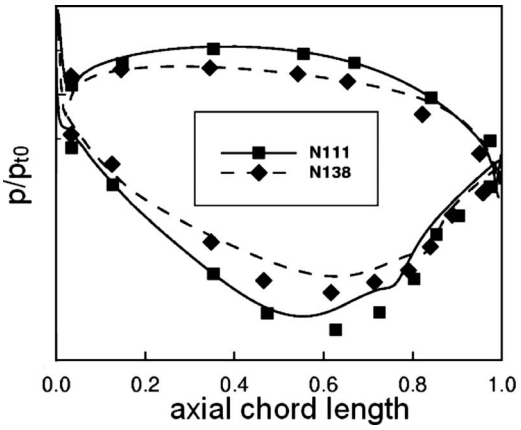

Fig. 11 Midspan surface pressure distribution for middle vane V2 in MTU-A turbine, comparison of baseline (N138) and high lift (N111), measurement (symbols), and CFD (lines)

ment variations this is almost constant for all measured pressure ratios. The build D01 with 111 vanes and two airfoils shows some sensitivity with respect to pressure ratio.

In the case of the 80% speed line the tendency between high lift and conventional lift is surprisingly reversed. Increasingly, with rising pressure ratio, the high lift build D02 exhibits a performance benefit up to 0.5%. This result is a strong indication of the major importance of the impact of the 3D losses with respect to lift variation. At the lower speed the turbine is running at stronger positive incidence. This is typical for this type of turbofan engines. At larger positive incidences the intensity of the losses due to 3D flow structures is increased due to the higher degree of turning and the stronger front loading of the pressure distribution. As mentioned above, build D02 was not only redesigned with higher lift vanes but also with additional 3D design features, which gained effectiveness with lower speeds and higher positive incidence, offsetting the detrimental effect of the high lift design.

The second important performance characteristic is the efficiency variation with Reynolds number. The Re lapse for the MTU-A rig is shown in Fig. 13. In this turbine the efficiency behaves in a similar fashion as the BR715 rig described above. At Re=550,000 the high lift build features the same efficiency as the conventional one. Toward lower Re numbers a significant efficiency drop up to 1% develops. At this point it should be mentioned, however, that the two lower Re numbers are below the design conditions. Interestingly the build D01 with the high lift vane 2 has the same efficiency drop for the lowest Re number, leading to the conclusion that this airfoil is at least close to separation.

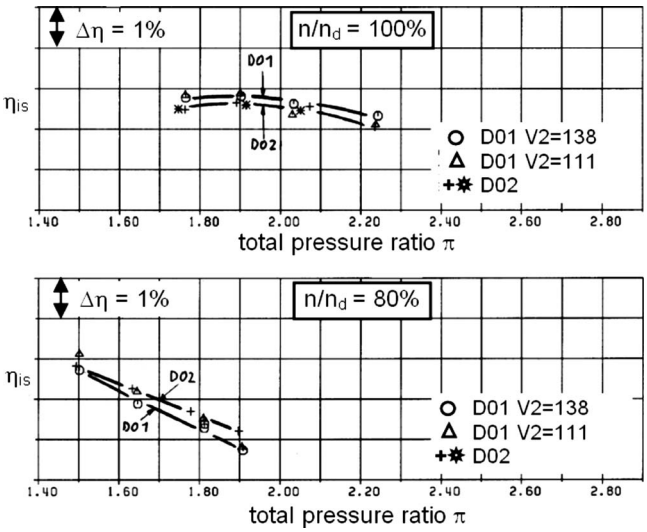

Fig. 12 Efficiency for 100% and 80% speed lines for MTU-A turbine, comparison of baseline D01, and high lift D02 builds

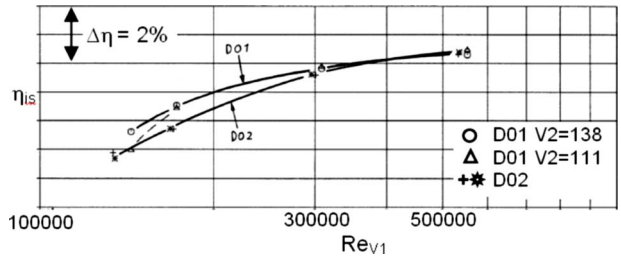

Fig. 13 Turbine efficiency versus Reynolds number (first vane) for MTU-A, comparison of baseline D01, D01_V2%–20%, and high lift D02 build, n/n_d=100%

The third rig in this discussion is a more recently tested large five-stage turbine (MTU-B). Two builds were tested with build B02 featuring high lift airfoils in seven of the ten turbine rows. The redesigned rows are colored in Fig. 14. In the modified rows the new loading was chosen at a Zweifel coefficient of about 1.15. Since the stage loading coefficient of this turbine is relatively high with a value above 2.5, this Zweifel level is already quite elevated. The Zweifel coefficient of the baseline build B01 varied to some extent. Hence, the airfoil lift increase is not identical for all redesigned rows. On average the airfoil count was reduced by approximately 25% in the modified rows.

The rig was heavily instrumented including static pressures on the vanes and intrarow pressure and temperature leading edge instrumentation. The tests were performed in the altitude test facility of Stuttgart University.

The efficiency as function of specific work and rotational speed is plotted in Fig. 15. Both experimental and numerical values computed with 3D CFD code TRACE in steady 3D mode are shown.

The introduction of the high lift airfoil rows produces an efficiency reduction of about 0.8% at design conditions, which is $\Delta h/T$=330 and 100% speed. At the design speed the original conventional lift turbine showed no efficiency variation with specific work, hence pressure ratio. However, the high lift turbine does show such sensitivity with decreasing efficiency with increasing work.

This trend is maintained for the 90% and 80% speed. At the lower speeds also the baseline turbine exhibits sensitivity with respect to specific work, but this is increased for the high lift arrangement. The reason for this behavior could be the 2D losses being more sensitive to pressure ratio driven Ma number change,

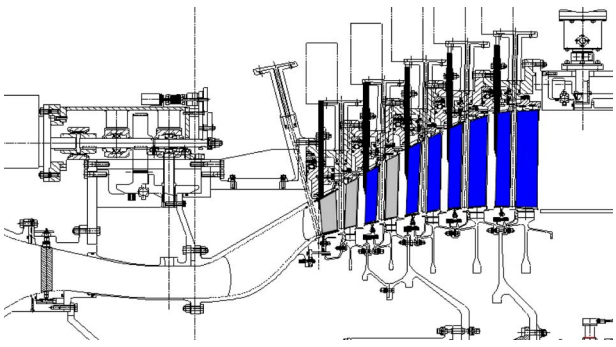

Fig. 14 General arrangement of five-stage rig, modified airfoil rows for build B02

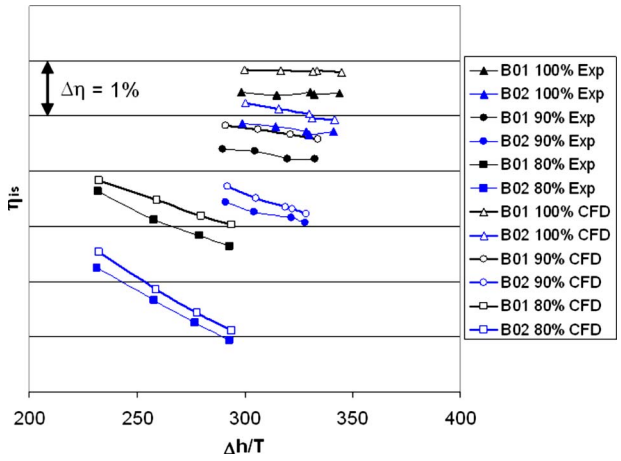

Fig. 15 Operating map of five-stage rig, comparison of build B01 and build B02

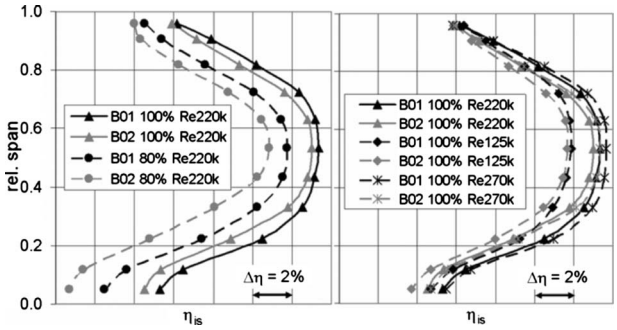

Fig. 17 Turbine efficiency versus span in MTU-B, sensitivity to speed (left), and Reynolds number (right)

as well as the 3D losses due to increased turning. It should also be highlighted at this point that the efficiency drop of the high lift versus the conventional lift doubles for the 80% speed compared with the design speed.

The first step in assessing the background for this behavior is to take a look at a typical pressure distribution. For this the fourth vane is chosen because it features a highly resolved pressure tapping in the suction side diffusion region at midspan (Fig. 16). The lift increase in this row is slightly below the average lift increase. From the pressure distribution plot the lift increase is clearly visible. In all three sections the peak suction has moved upstream with the throat area. In order to avoid too high peak Mach numbers and suction side diffusion rates, the pressure distribution is designed with more forward loading.

Taking a closer look into the 50% span distribution it can be seen that the separation bubble has moved upstream in the high lift airfoil. This goes in line with a longer turbulent boundary layer length. The result is a loss increase at midspan, similar to the findings in the cascades. For the entire turbine this loss increase at midspan can be seen in the radial efficiency distribution plotted in Fig. 17.

In the left plot of this figure an efficiency difference between B01 and B02 at midspan of about 0.35% is present for design conditions. The overall efficiency drop for this operating point is 0.8%. As can also be seen from the same plot the additional losses originate in the endwall regions, thus can be attributed to the 3D loss mechanisms discussed in the cascade section above. Actually, these 3D losses are further increased through the additional losses of the leakage flows (for further background on leakage related loss see Ref. [45]). Although the velocity triangles are not changed through the introduction of high lift, the circumferential nonuniformities cause additional mixing grow with increasing lift.

In Fig. 18 the secondary kinetic energy distribution from the CFD computation is shown for two operating conditions. At design condition this quantity increases by approximately 25%. Both hub and tip endwall regions are subject to this increase. Although SKE does not necessarily directly translate into loss, it is a strong indication of intensified secondary flow structures. Since the underlying CFD has been run omitting leakage, this effect can be expected to be even stronger in the real machine. And as discussed above there are additional losses due to a higher local Ma number level on the endwalls.

At 80% speed the efficiency at midspan is reduced by 0.9%. This indicates that the midspan loss increase at this off-design condition is overproportional. However, the 3D loss increase is obviously even stronger. One indication is pure arithmetics: The additional efficiency loss due to 3D effects at design point conditions is 0.8–0.35=0.45%, while at 80% speed this value is 1.6–0.9=0.7%. Another characteristic change is the shape of the radial efficiency distribution. In both operating points, but especially at 80% speed the high lift turbine has a thinner region of higher efficiencies at midspan (Fig. 17). This is a good indication of the stronger secondary flows and happens because the larger pitch to chord ratio leads to radially enlarged vortices. This is also in line with Fig. 18. At 80% speed the total SKE magnitude is comparable to the 100% speed (higher at the hub, lower at the tip) but for a smaller pressure ratio, thus a smaller velocity level.

It should be also mentioned here, that the CFD computation (TRACE) did a quite good job in predicting the flow. The pressure distribution is well reproduced including the separation bubbles for all three spanwise locations and reduced speed. One reason for this also is actually the excellent hardware quality of the milled airfoils. This enables to reproduce the operating lines quite well too (Fig. 15).

On the right side of Fig. 17 the design efficiency distribution is compared with a lower and a higher Re number. Actually, the higher Re number is not a take-off condition due to power limitations of the facility. The midspan efficiency penalty for the high

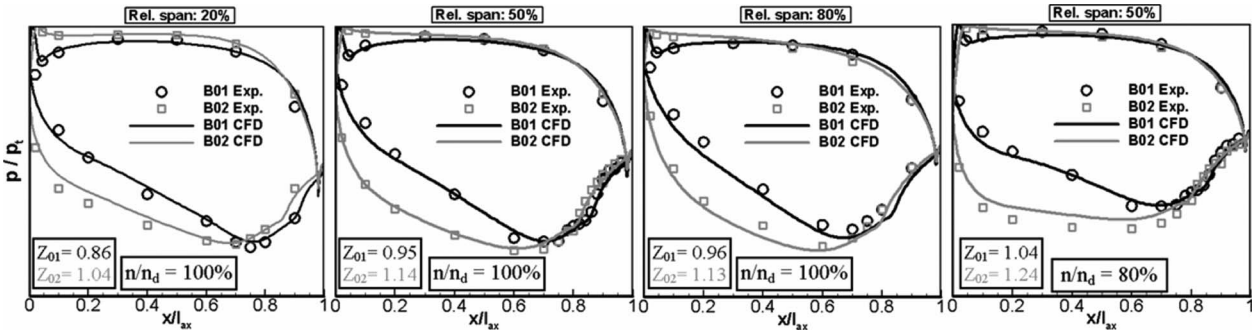

Fig. 16 Surface pressure distribution for Rig MTU-B, Vane 4, for 100% speed and 80% speed, Re=design

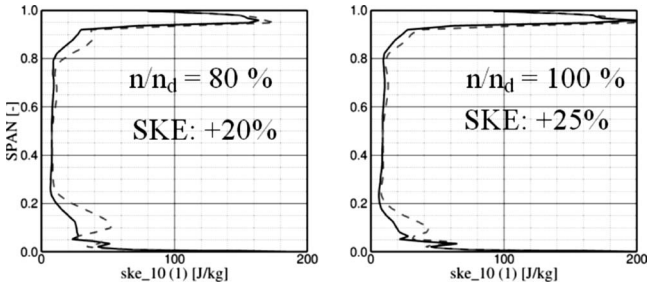

Fig. 18 Secondary kinetic energy change for MTU-B, V4, reference B01 black, high lift B02 light

lift is only 0.2% for the low Re number compared with 0.3–0.35 for the two higher Re numbers. This is interesting, since usually one would expect a stronger Re lapse for the high lift at midspan. Also the efficiency drops more in the hub than in the tip region for the high lift configuration. This could be partly due to the mild change in the radial vortexing, which was necessary for the high lift introduction at the hub. Another reason could be a more intensive interaction of the suction side boundary layer with the secondary flow.

In Fig. 19 the integral efficiency is plotted versus Reynolds number for measurement and CFD. The CFD provides a reasonably good prediction with a little bit of improvement potential for B02 at the high Re number. The design condition is at Re=220k, which is the first vane Re number. At this operating point the last vane runs at about Re=100k.

The significant difference with both MTU-A and the BR715 rig is the Re lapse rate. In this MTU-B rig the efficiency reduction due to high lift is larger for the higher Reynolds number than for the smallest one. And this phenomenon is smooth, i.e., the intermediate Re numbers exhibit intermediate efficiency effects. Again it should be noted here that an operating point near take-off, the Re number could not be measured due to the size of the rig. So, a direct comparison with the BR715 cannot be made in this respect.

The question is, what causes this rig to behave differently with respect to Re lapse. The question has not been answered completely yet. However, the type of pressure distribution used in the MTU-B rig is somewhere between the two high lift cascades from the previous chapter (T161 and T162). And these showed a quite different Re lapse behavior. A second reason could be the intensification of the individual wakes, which triggers an earlier and more stable transition location on the subsequent airfoil row. As mentioned above the efficiency penalty of the high lift build B02 at midspan is 0.2% for the lowest Re number and 0.35% at the design Re number. This is quite exactly also the integral efficiency

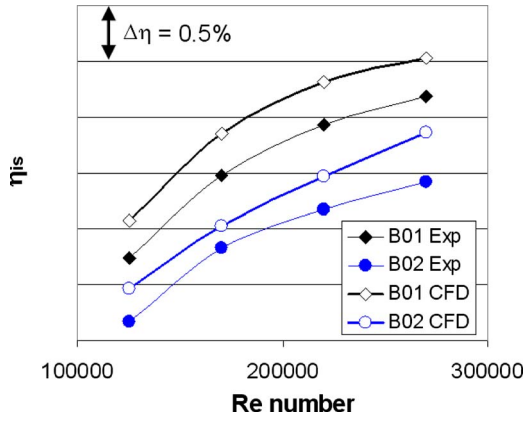

Fig. 19 Reynolds lapse of five-stage rig, comparison of build B01 and build B02

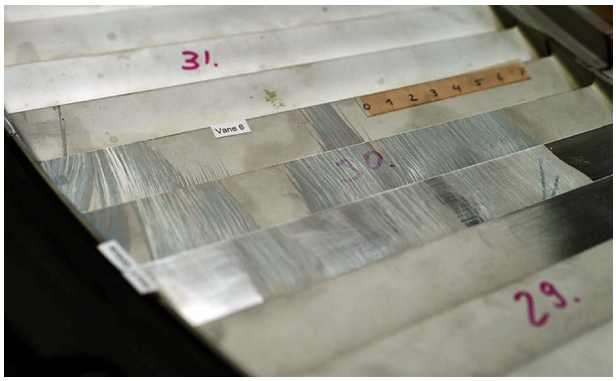

Fig. 20 Flow visualization in fourth vane, rig MTU-B

delta variation between the two Re numbers. This provides a strong indication that the 2D loss mechanisms play the larger role for this.

In Fig. 20 a photograph of the fourth vane with dye injection is shown. Although this vane already runs at Re numbers not much larger than 100k in the design point, no recirculation zone on the suction side representing a separation could be found. From this one could deduce that the more intensive wakes in connection with the longer surface length downstream of the throat play a major role for the reduced Re lapse. This may have been amplified through the relatively high stage loading coefficient leading to elevated surface Ma number and the connected large flow turning in the airfoil rows.

5 Path to Optimal Choice of Airfoil Lift Level

In Secs. 3 and 4 a lot of results of high lift investigations have been described and discussed. The question is what can be learned from this with respect to an optimal choice of the airfoil lift. As mentioned in the beginning, the overall trade has to be done together with weight and cost. Since this trade very much depends on a lot of topics, such as airplane, typical mission, etc., the optimal trade will vary but will always be at a higher lift level than the lift for optimal efficiency only.

In Secs. 3 and 4 a couple of main insights have been gathered. Both 2D and 3D losses contribute to a loss increase of high lift airfoils. The difference is that for 2D losses there is an optimal airfoil load, while for the 3D losses there is no mechanism, which ends up having a minimal loss contribution at reasonable Zweifel coefficients.

The diagram of Denton [41] for optimal pitch to chord ratio translated into optimal Zweifel coefficient for a typical LP turbine velocity triangle (T106) would give an optimal Zweifel number somewhere in the proximity of 0.9. Interestingly this still in the range of loading coefficients given by Zweifel [1] himself in 1945. Although this number is based on an estimation of a constant diffusion coefficient, which is not reality in transitional LP turbine boundary layers, this result seems reasonable. However, adding the impact of the 3D losses, which gradually increase with increasing airfoil loading, the optimum including both effects has to move to smaller airfoil loadings.

Some measures can be taken to move the optimum airfoil loading to higher levels. The first is to do an appropriate airfoil design, i.e., pressure distribution. This may have a significant impact, as shown above and in literature. The choice of this design has to take some important boundary conditions into account, such as flight altitudes, stage loading, stage pressure ratio, operating range, and annulus shape.

In addition, introducing measures for reduction in secondary flow intensity, such as 3D airfoil design and endwall contouring, e.g., Praisner et al. [46] will have more effect for larger airfoil loading and will thus also move the optimum Zweifel coefficient

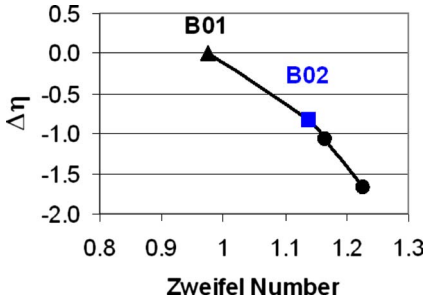

Fig. 21 Efficiency drop predicted by CFD for MTU-B turbine for designs with different average Zweifel coefficients

to higher levels. Further improvement may come from additional measures for boundary layer control. By this the purely aerodynamic optimum airfoil load may be driven to Zweifel numbers in the area of 1.0 for conventional LP turbines. Turbines with a high stage loading feature optimum lift levels of about 0.1 less in terms of Zweifel number due to their elevated Mach number levels.

However, there is no physical reason for a large flat region of constant efficiency for varying airfoil load. Even in the absence of any open separations or similar drastic flow effects the pure Mach number driven increase in 2D and especially 3D losses cannot be avoided.

In order to determine the optimum airfoil lift level for a given LP turbine application, the designer first has to use good experience based predesign programs to determine the appropriate range of airfoil lift. And following this he needs a well validated and reliable 3D CFD code for the exact choice of airfoil lift and the evaluation of the detailed design.

The last figure of this paper (Fig. 21) is taken from the CFD based design of the MTU-B high lift turbine. It shows the computed efficiency of the baseline turbine, the finally chosen build B02, and two fully aerodesigned versions with even higher lift coefficients. Although it is not complete in the sense that no lift levels below the datum turbine have been designed, it gives some indication that the baseline design is aerodynamically already on the high side with respect to airfoil lift level.

6 Conclusions

In this paper investigations on the impact of aerodynamic airfoil loading on loss and efficiency are described and summarized. The continuously growing literature on the topic of increasing the airfoil lift lays out a good basis for such development. However, most of the related research has been performed in cascade tests, and only limited information about the trends in real machinery has been available so far.

The discussion focuses on assessment of loss sensitivities with varying airfoil lift. For this, cascade data are evaluated first. Following this evaluation, investigations on three test turbines are discussed. It turns out that most of the behavior of the turbine flow can be explained by the basic considerations. However, as could be expected, the relative magnitude of the loss determining mechanisms is different between the different turbine configurations. One example is that the Reynolds lapse rate does not have to be steeper for higher lift designs.

Evaluating the overall picture of efficiency sensitivity with respect to airfoil lift, it is concluded that a distinct lift exists for optimum efficiency. With respect to the dimensionless Zweifel coefficient as a measure for airfoil lift this optimum is located somewhere in the range between 0.8 and 1.0 for typical LP turbines depending on the aerodynamic boundary conditions and blade design limitations. Increasing the lift further inevitably will lead to progressively reduced efficiencies.

There are measures to move the aero-optimal lift level to larger values. This could be done by boundary layer control to reduce 2D losses especially at lower Reynolds numbers and through introduction of suitable 3D design to reduce endwall flow related losses.

The optimal airfoil lift level is of course somewhat higher for an aero-engine turbine because the savings in weight and cost with fewer airfoils per row trade into this direction. This actual number for this optimal lift depends strongly on the mission of the airplane and the related trades.

Acknowledgment

The authors wish to thank MTU Aero Engines for permission to publish this paper. They also want to acknowledge Mr. Timo Merenda and Thomas Germain, who assisted in preparing some of the paper figures. Furthermore the authors would like to thank for the partial funding of the projects through the Luftfahrtforschungsprogramm phase 1 and 3.

Nomenclature

A = area (m^2)
c = chord (m)
C_d = diffusion coefficient
C_s = surface length (m)
Cp = pressure coefficient
h = enthalpy (kJ/kg)
h = airfoil height (m)
l = true chord (m)
l_{ax} = axial chord (m)
m = mass flow rate (kg/s)
P, p = pitch (m)
p = pressure (Pa)
S = entropy generation rate (kg m/s^3 K)
T = temperature (K)
V = velocity (m/s)
V_0 = velocity at boundary layer edge (m/s)
x = axial coordinate (m)
w = velocity in relative frame (m/s)
Z = Zweifel coefficient
Ma = Mach number
Re = Reynolds number
PS = pressure side
SS = suction side
α = flow angle (from axis) (deg)
β_S = stagger angle (deg)
η = efficiency
γ = isentropic coefficient
π = pressure ratio
ρ = density (kg/m^3)
ζ = loss coefficient

Subscripts

ax = axial
is = isentropic
m = meridional
s = entropy
0 = total
1 = inlet
2 = exit

References

[1] Zweifel, O., 1945, "Die Frage der optimalen Schaufelteilung bei Beschaufelungen von Turbomaschinen, insbesondere bei großer Umlenkung in den Schaufelreihen," Brown Boveri Rev., **32**(12), pp. 436–444.
[2] Emmons, H. W., 1951, "The Laminar-Turbulent Transition in a Boundary Layer–Part I," J. Aerosp. Sci., **18**, pp. 490–498.
[3] Schubauer, G. B., and Klebanoff, P. S., 1955, "Contributions on the Mechanics of Boundary Layer Transition," NACA TN 3489 (1955) and NACA Report No. 1289. (1956).
[4] Walker, G. J., 1974, "The Unsteady Nature of Boundary Layer Transition on an Axial-Flow Compressor Blade," ASME Paper No. 74-GT-135.
[5] Hodson, H. P., 1984, "Boundary Layer and Loss Measurements on the Rotor

of an Axial Flow Turbine," ASME J. Eng. Gas Turbines Power, **106**(2), pp. 391–399.
[6] Hodson, H. P., Huntsman, I., and Steele, A. B., 1994, "An Investigation of Boundary Layer Development in a Multistage LP Turbine," ASME J. Turbomach., **116**, pp. 375–383.
[7] Halstead, D. E., Wisler, D. C., Okiishi, T. H., Walker, G. J., Hodson, H. P., and Shin, H., 1997, "Boundary Layer Development in Axial Compressors and Turbines—Part 1: Composite Picture," ASME J. Turbomach., **119**(1), pp. 114–127.
[8] Halstead, D. E., Wisler, D. C., Okiishi, T. H., Walker, G. J., Hodson, H. P., and Shin, H., 1995, "Boundary Layer Development in Axial Compressors and Turbines—Part 2: Compressors," ASME J. Turbomach., **119**(3), pp. 426–444.
[9] Halstead, D. E., Wisler, D. C., Okiishi, T. H., Walker, G. J., Hodson, H. P., and Shin, H., 1995, "Boundary Layer Development in Axial Compressors and Turbines—Part 3: LP Turbines," ASME J. Turbomach., **119**(2), pp. 225–237.
[10] Halstead, D. E., Wisler, D. C., Okiishi, T. H., Walker, G. J., Hodson, H. P., and Shin, H., 1997, "Boundary Layer Development in Axial Compressors and Turbines—Part 4: Computations and Analyses," ASME J. Turbomach., **119**(1), pp. 128–139.
[11] Hoheisel, H., Kiock, R., Lichtfuss, H. J., and Fottner, L., 1987, "Influence of Free-Stream Turbulence and Blade Pressure Gradient on Boundary Layer and Loss Behaviour of Turbine Cascades," ASME J. Turbomach., **109**, pp. 210–219.
[12] Hourmouziadis, J., 1989, "Aerodynamic Design of Low Pressure Turbines," ASME Paper No. AGARD-LS-167.
[13] Pfeil, H., Herbst, R., and Schröder, Th., 1983, "Investigation of Laminar-Turbulent Transition of Boundary Layers Disturbed by Wakes," ASME J. Turbomach., **105**, pp. 130–137.
[14] Hodson, H. P., 1990, "Modelling Unsteady Transition and Its Effects on Profile Loss," ASME J. Turbomach., **112**(4), pp. 691–701.
[15] Schulte, V., and Hodson, H. P., 1998, "Unsteady Wake-Induced Boundary Layer Transition in High Lift LP Turbines," ASME J. Turbomach., **120**(1), pp. 28–35.
[16] Banieghbal, M. R., Curtis, E. M., Denton, J. D., Hodson H. P., Huntsman, I., Schulte, V., Harvey, N. W., and Steele, A. B., 1995, "Wake Passing in LP Turbines," AGARD Conference on Loss Mechanisms and Unsteady Flows in Turbomachines, Derby, UK, May, Paper No. 23.
[17] Stadtmüller, P., Fiala, A., and Fottner, L., 2000, "Experimental and Numerical Investigation of Wake-Induced Transition on a Highly Loaded LP Turbine at Low Reynolds Numbers," ASME Paper No. 2000-GT-269.
[18] Gier, J., Ardey, S., Heisler, A., 2000, "Analysis of Complex Three-Dimensional Flow in a Three-Stage LPT by Means of Transitional Navier-Stokes Simulation," ASME Paper No. 2000-GT-0645.
[19] Gier, J., and Ardey, S., 2001, "On the Impact of Blade Count Reduction on Aerodynamic Performance and Loss Generation in a Three-Stage LP Turbine," ASME Paper No. 2001-GT-0197.
[20] Ardey, S., and Gier, J., 2001, "Randzonenbeeinflussung bei Schaufelzahlreduktion in Niederdruckturbinen," Paper No. DGLR-2001-206.
[21] Haselbach, F., Schiffer, H. P., Horsmann, M., Dressen, S., Harvey, N. W., and Read, S., 2002, "The Application of Ultra High Lift Blading in the BR715 LP Turbine," ASME J. Turbomach., **124**(1), pp. 45–51.
[22] Howell, R. J., Hodson, H. P., Schulte, V., Stieger, R. D., Schiffer, H. P., Haselbach, F., and Harvey, N. W., 2002, "Boundary Layer Development in the BR710 and BR715 LP Turbines–The Implementation of High Lift and Ultra–High–Lift Concepts," ASME J. Turbomach., **124**, pp. 385–392.
[23] Houtermans, R., Coton, T., and Arts T., 2003, "Aerodynamic Performance of a Very High Lift LP Turbine Blade With Emphasis on Separation Prediction," ASME Paper No. GT-2003-38802.
[24] Coton, T., and Arts, T., 2004, "Investigation of a High Lift LP Turbie Blade Submitted to Passing Wakes—Part 1: Profile Loss and Heat Transfer," ASME Paper No. GT2004-53768.
[25] Coton, T., and Arts, T., 2004, "Investigation of a High Lift LP Turbie Blade Submitted to Passing Wakes—Part 2: Boundary Layer Transition," ASME Paper No. GT2004-53781.
[26] Popovic, I., Zhu, J., Dai, W., Sjolander, S. A., Praisner, T., and Grover, E., 2006, "Aerodynamics of a Family of Three Highly Loaded Low-Pressure Turbine Airfoils: Measured Effects of Reynolds Number and Turbulence Intensity in Steady Flow," ASME Paper No. GT2006-91271.
[27] Praisner, T. J., Allen-Bradley, E., Knezevici, D. C., Sjolander, S. A., and Grover, E. A., 2007, "Application of Non-Axisymmetric Endwall Contouring to Conventional and High-Lift Turbine Airfoils," ASME Paper No. GT2007-27579.
[28] Lazaro, B. J., Gonzalez, E., and Vazquez, R., 2007, "Unsteady Loss Production Mechanisms in Low Reynolds Number, High Lift, Low Pressure Turbine Profiles," ASME Paper No. GT2007-28142.
[29] MTU, 1987, "Axial durchströmtes Schaufelgitter einer mit Gas oder Dampf betriebenen Turbine," European Patent No. EP 0 132 638 B1.
[30] Sitaram, N., Govardhan, M., and Krishna, V. T., 1999, "Loss Reduction by Means of Two-Dimensional Roughness Elements on the Suction Surface of a Linear Turbine Rotor Cascade," Flow, Turbul. Combust., **62**(3), pp. 227–248.
[31] Volino, R. J., 2003, "Passive Flow Control on Low-Pressure Turbine Airfoils," ASME Paper No. GT2003-38728.
[32] Ramesh, O. N., Hodson, H. P., and Harvey, N. W., 2001, "Separation Control in Ultra-High Lift Aerofoils by Unsteadiness and Surface Roughness," 15th International Symposium on Air Breathing Engines, Bangalore, India, Sept.
[33] Zhang, X. F., Vera, M., Hodson, H., and Harvey, N., 2006, "Separation and Transition Control on an Aft-Loaded Ultra-High-Lift LP Turbine Blade at Low Reynolds Numbers: Low-Speed Investigation," ASME J. Turbomach., **128**(3), pp. 517–527.
[34] Vera, M., Zhang, X.-F., Hodson, H.P., and Harvey, N.W., 2007, "Separation and Transition Control on an Aft-Loaded Ultra-High-Lift LP Turbine Blade at Low Reynolds Numbers: High-Speed Validation," ASME J. Turbomach., **129**(2), pp. 340–347.
[35] Bons, J., Sondergard, R., and Rivir, R., 2001, "Control of Low-Pressure Turbine Separation Using Vortex Generator Jets," ASME J. Turbomach., **123**, pp. 198–206.
[36] Sondergard, R., Bons, J., Sucher, M., and Rivir, B.: 2002, "Reducing Low-Pressure Stage Blade Count Using Vortex Jet Separation Control," ASME Paper No. GT-2002-30602.
[37] Volino, R. J., 2003, "Separation Control on Low-Pressure Turbine Airfoils Using Synthetic Vortex Generator Jets," ASME Paper No. GT2003-38729.
[38] McAuliffe, B. R., and Sjolander, S. A., 2004, "Active Flow Control Using Steady Blowing for a Low-Pressure Turbine Cascade," ASME J. Turbomach., **126**(4), pp. 560–569.
[39] Pullan, G., and Harvey, N. W., 2006, "The Influence of Sweep on Axial Flow Turbine Aerodynamics at Mid-Span," ASME Paper No. GT2006-91070.
[40] Traupel, W., 2000, *Thermische Strömungsmaschinen*, Vol. 1, Springer Verlag, Auflage, Berlin, p. 4.
[41] Denton, J. D., 1993, "Loss Mechanisms in Turbomachines," ASME J. Turbomach., **115**, pp. 621–656.
[42] Hoheisel, H., 1985, "Zusatzuntersuchungen an den Turbinengittern T107 und T106 mit Variation der Schaufelteilung," DFVLR, Report No. IB 129-85/30.
[43] Kozulovic, D., Röber, T., and Nürnberger, D., 2007, "Application of a Multimode Transition Model to Turbomachinery Flows," *Proceedings of the Seventh European Turbomachinery Conference*, Athens, Greece.
[44] Zoric, T., Popovic, I., Sjolander, S. A., Praisner, T., Grover, E., 2007, "Comparative Investigation of Three Highly Loaded LP Turbine Airfoils—Part 1: Measured Profile and Secondary Losses at Design Incidence," ASME Paper No. GT2007-27537.
[45] Gier, J., Stubert, B., Brouillet, B., and de Vito, L., 2005, "Interaction of Shroud Leakage Flow and Main Flow in a Three-Stage LP Turbine," ASME J. Turbomach., **127**, pp. 649–658.
[46] Praisner, T. J., Allen-Bradley, E., Grover, E. A., Knezevici, D. C., and Sjolander, S. A., 2007, "Application of Non-Axisymmetric Endwall Contouring to Conventional and High-Lift Turbine Airfoils," ASME Paper No. GT2007-27579.